Dual topology and versatile Rashba-split surface state configurations in 2M-phase WS_2 and WSe_2

Lixuan Xu[1,2], Yuqiang Fang[3], Fuqiang Huang[3], Shihao Zhang[4], Shiheng Liang[1,2], Yulin Chen[5,6,7], Lexian Yang[8], Zhongkai Liu[5,6], Nan Xu[9,10] and Yiwei Li[9*]

[1]*Department of Physics, Hubei University, Wuhan 430062, China*

[2]*Key Laboratory of Intelligent Sensing System and Security (Hubei University), Ministry of Education, Wuhan 430062, China*

[3]*School of Materials Science and Engineering, Shanghai Jiao Tong University, Shanghai 200240, China*

[4]*School of Physics and Electronics, Hunan University, Changsha 410082, China*

[5]*School of Physical Science and Technology, ShanghaiTech University, Shanghai 201210, China*

[6]*ShanghaiTech Laboratory for Topological Physics, Shanghai 201210, China*

[7]*Department of Physics, University of Oxford, Oxford OX1 3PU, UK*

[8]*State Key Laboratory of Low Dimensional Quantum Physics, Department of Physics, Tsinghua University, Beijing 100084, China*

[9]*Institute for Advanced Studies (IAS), Wuhan University, Wuhan 430072, China*

[10]*Wuhan Institute of Quantum Technology, Wuhan 430206, China*

**yiweili@whu.edu.cn*

Abstract

2M-phase transition metal dichalcogenides have recently attracted intensive research interest due to their rich topological and superconducting phase diagrams. Apart from the topological surface states of 2M-WS_2 near Γ originated from the strong topological order, using angle-resolved photoemission spectroscopy, we discover additional Rashba-split states on the surfaces of both 2M-WS_2 and 2M-WSe_2, which extend in large momentum-energy regions. First-principles calculations well reproduce these states and attribute them to the weak topological orders. The calculations further indicate that the surface state connecting configurations are tunable under moderate pressure, suggesting that 2M-WS_2 and WSe_2 are promising platforms to study topological phase transition and explore topological superconductivity.

To realize topological superconductivity (TSC) based on the Fu-Kane model, the key ingredient is to introduce superconductivity on spin-helical states [1], such as topological boundary states of topological materials or Rashba-split states (RSS) of semiconductors due to combined effect of spin-orbit coupling (SOC) and broken inversion symmetry of the crystal field. In this approach, the superconducting phase is realized either on the interface of designed heterostructures by the proximity effect [2–6] or, more effectively, on the surface of intrinsic superconducting topological materials by the self-proximity effect [7–11]. Various candidate materials of the latter category have been recently proposed, including Cu-intercalated Bi_2Se_3 [7], iron-based superconductors [8,9], and 2M-WS_2 [10,11], and experimental signatures of Majorana quasiparticles have been identified, such as superconducting topological surface states (TSS) [8,11] and zero-bias conductance peak [9,10].

TSC candidate 2M-WS_2 belongs to the 2M-phase transition metal dichalcogenide (TMDC) family [12]. This material family has exhibited rich superconducting and topological phase diagrams [13–17]. 2M-WS_2 hosts the highest superconducting transition temperature T_C = 8.8 K among all TMDC under ambient pressure [18]. Topological classifications indicate that 2M-phase WS_2 and WSe_2 are in the strong and weak categories, respectively [16]. The diverse topological properties imply that 2M-TMDC might realize dual topological orders and provide superconducting material platforms with tunable TSS.

In this letter, by using angle-resolved photoemission spectroscopy (ARPES) and first-principles calculations, we discover topological RSS on the naturally cleaved (100) surfaces of both 2M-phase WS_2 and WSe_2, which are associated with the weak topological orders. In contrast to TSS in conventional topological insulators like Bi_2Se_3 and Bi_2Te_3 [19–21], these states are derived from Shockley states under finite SOC, similar to the scenario on the (111) surface of grey arsenic [22]. Compared to the well-studied TSS of 2M-WS_2 residing in a small momentum-energy region near Γ ($\Delta k < 0.1$ Å^{-1}, $\Delta E < 100$ meV) [11,23], the newly discovered topological RSS extends in momentum-energy space ($\Delta k > 0.6$ Å^{-1}, $\Delta E > 1$ eV). Our calculations further reveal that topological and trivial RSS can switch under moderate pressure. Hence, 2M-phase WS_2 and WSe_2 might provide an ideal platform to explore TSC with tunable spin-split surface state connecting configurations.

High-quality single crystals of 2M-phase WS_2 and WSe_2 were synthesized by the deintercalation of interlayer potassium cations from K_xWS_2 and K_xWSe_2 crystals. The synchrotron-ARPES measurements were performed at beamline BL07U of Shanghai Synchrotron Radiation Facility (SSRF), China, with a photon energy of 94 eV [24], and Beamline 5-2 of Stanford Synchrotron Radiation Lightsource (SSRL), using photon energies from 28 eV to 90 eV [25]. The laser-ARPES measurements were performed at a lab-built facility at ShanghaiTech University delivering 6.994-eV photons. For all ARPES measurements, the samples were cleaved *in situ* along the (100) plane and measured under high vacuum below 5×10^{-11} Torr using a ScientaOmicron DA30-L analyzer. The measurement temperature was kept between 15 K to 20 K. Linear-horizontal (LH) polarized photons were used in ARPES measurements. The first-principles calculations were carried out via the Vienna *ab initio* simulation package (VASP) [26]. The exchange-correlation energy was approximated by the Perdew-Burke-Ernzerhof (PBE) type generalized gradient approximation (GGA) [27]. Topological properties, including surface state calculations, were performed with WannierTools package [28], based on the tight-binding Hamiltonians constructed from maximally localized Wannier functions (MLWFs) by the Wannier90 package [29–31]. In addition, calculations based on the local density approximation [32] plus an on-site Hubbard U (LDA+U), PBE plus an on-site Hubbard U (PBE+U), the modified Becke-Johnson (mBJ) functional [33], and Heyd-Scuseria-Ernzerhof (HSE) hybrid functional [34] were performed to confirm the assignment of the bulk and surface states, as well as the surface state connecting configurations that are related to the topological property [35].

Tungsten dichalcogenides have three types of crystalline structures: the semiconducting 2H- and 3R-phases [36], and the metallic 2M-phases. 2M-WS_2 and WSe_2 crystallize in a base-centered monoclinic unit cell (space group No. 12, C2/m), which can be regarded as translationally stacked 1T' quantum spin Hall layers along the [100] direction [16], as shown in Fig. 1(a). The bulk Brillouin zone (BZ) and the (100) surface BZ are shown in Fig. 1(b).

First-principles calculated bulk band structures of 2M-phase WS_2 and WSe_2 confirm their metallic nature, with the α and β bands crossing the Fermi level [Figs. 1(c) and 1(d)]. The inclusion of SOC forbids band crossings and thus lead to band gaps at any arbitrary momentum.

For topological property analysis, 2M-WS_2 and 2M-WSe_2 exhibit a strong topological order [Z_2 = (1, 000)] and a weak topological order [Z_2 = (0, 100)], respectively, if the curved Fermi level is placed between the α and β bands. These distinct topological properties, which have been confirmed by ARPES studies, are jointly determined by the band inversion amplitude and interlayer coupling [11,16].

We further discover that 2M-WS_2 and 2M-WSe_2 host a weak topological order [Z_2 = (0, 001)] if the curved Fermi level is between the β and γ bands. One should note that this weak topological order is distinct from that between the α and β bands of 2M-WSe_2. The weak indices indicate that the naturally cleaved (100) surface is the topologically dark "top" surface between the α and β bands, whereas it is the "side" surface between the β and γ bands, hosting an even number of surface Dirac cones in a surface BZ. Figures 1(e) and 1(f) illustrate possible (100) surface state connection configurations for 2M-WS_2 and WSe_2, respectively, which are constrained by their topological invariants [37].

Surface-projected band calculations of 2M-WS_2 and 2M-WSe_2 reveal the bulk continuum of the α, β and γ bands, as shown in Figs. 2(a) and (c). Consistent with our topological order analysis, we identify a single surface Dirac cone (TSS1) near $\bar{\Gamma}$ between the α and β bands of 2M-WS_2, and two surface Dirac cones (TSS2 and TSS3) centered at $\bar{Y}$ and $\bar{R}$ between the β and γ bands of both 2M-WS_2 and 2M-WSe_2. ARPES measurements covering the whole BZ show consistent bulk band dispersions with the calculation [Figs. 2(b) and (d)]. The α, β and γ bands are unambiguously resolved by ARPES, however, the band gaps between the β and γ bands near $\bar{Y}$ and $\bar{R}$ are smeared out possibly due to large self-energies at high binding energies.

Fine ARPES measurements of 2M-WS_2 and 2M-WSe_2 reveal the signatures of the expected TSS, as shown in Figure 3. To clearly observe TSS1, we performed laser-ARPES on the surface potassium (K) doped 2M-WS_2 along the $\bar{Y} - \bar{\Gamma} - \bar{Y}$ direction, as shown in Fig. 3(a). The α band and TSS1 are well resolved and consistent with the calculation [Fig. 3(b)] and previous studies [11,16,17,23]. TSS1 resides in a local band gap with a small momentum-energy region near $\bar{\Gamma}$ ($\Delta k < 0.1$ Å^{-1}, $\Delta E < 100$ meV).

Band dispersions along the $\overline{Y} - \overline{\Gamma} - \overline{Y}$ direction of 2M-WS_2 and 2M-WSe_2 in a larger momentum-energy region are measured by synchrotron-ARPES, as shown in Figs. 3(c) and 3(e). The second-derivative plots show nice consistency with corresponding calculations [Figs. 3(d) and 3(f)]. We clearly observe two branches of TSS2 and they merge into the β and γ bulk continuums, respectively, manifesting their nontrivial topology [38]. The dispersions of these TSS can also be well traced by peaks of momentum-distribution-curves and energy-distribution-curves [35]. The assignment of the bulk bands and TSS is confirmed by photon-energy-dependent ARPES measurements and first-principles calculations [35].

TSS2 shows distinct properties compared to TSS in conventional topological insulators, such as Bi_2Se_3 and Bi_2Te_3 [19–21]. They expand in both energy and momentum directions ($\Delta k >$ 0.6 $Å^{-1}$, $\Delta E >$ 1 eV). They are derived from Shockley surface states due to band inversions and their existence is guaranteed before the SOC is included [35]. As shown in Fig. 4(a), the spin-degenerated Shockley surface states can evolve into a pair of RSS, however, their connecting configurations are determined by the bulk band topology [35]. The upper and lower branches of topological RSS are connected to conduction and valence bulk continuums, respectively, whereas trivial RSS are connected to either conduction or valence bulk continuums.

Because the two-fold rotational symmetry and inversion symmetry are both broken in the surface state, the symmetry-allowed spin-orbital coupling contributes to Rashba-like splitting and spin textures of the surface state, as elaborated in the Supplemental Material [35]. Surface-projected band calculations of 2M-WSe_2 indicate that the connecting configurations of RSS centered at time-reversal invariant momenta $\overline{Y}$, $\overline{R}$, and $\overline{X}$ evolve under pressure, as shown in Figs. 4(b) and 4(c). The topological order between the β and γ bands transit from Z_2 = (0, 001) with a nonzero weak topological index under zero pressure to Z_2 = (1, 001) with a nonzero strong topological index under 4-GPa pressure. Consequently, topological and trivial RSS switch and the number of topological RSS pairs change from even (2) under zero pressure ($\overline{Y}$ and $\overline{R}$) to odd (1) under 4-GPa pressure ($\overline{X}$). The connecting configurations of RSS of 2M-WS_2 follow the same evolution trend under pressure as those of 2M-WSe_2 [35]. We call for further investigations using ARPES with *in situ* strain [39,40], which might provide experimental signatures on these versatile connecting configurations of RSS.

To effectively achieve a spinless *p*-wave superconductor based on RSS, delicate conditions associated with SOC, chemical potential, Zeeman coupling and superconducting gaps are required [5]. 2M-phase WS_2 and WSe_2 are van der Waals TMDC and their carrier density can be tuned through liquid gating [14] or chemical doping [15]. The RSS of interest cover a large energy range near the Fermi level and their topological properties are tunable with pressure. Their superconducting properties also evolve with pressure [41,42] and thus can lead to a rich phase diagram consisting of novel quantum states and require further investigations.

The discovery of TSS2 in 2M-WS_2 and 2M-WSe_2 broadens the material family with dual topology and may open the possibility to applications based on surface states with distinct topological properties. Materials with dual topology can host rich spin-helical surface states, however, candidates with superconducting phases are extremely rare [43-49]. The most prominent examples are iron-based superconductors that exhibit both topological insulator and Dirac semimetal states near the Fermi energy [43]. However, other superconducting dual topological candidates either host extremely low T_C [50] or lack experimental evidence [48]. In contrast, pristine 2M-WS_2 and pressurized 2M-WSe_2 exhibit relatively high T_C of 8.8 K [11,18] and 7.3 K [41], respectively. Therefore, we propose that these superconducting compounds with dual topology might provide a versatile platform to explore TSC with distinct configurations of RSS.

The authors acknowledge generous assistance from Cheng Chen, Yu He, Donghui Lu and Makoto Hashimoto during the beam time at SSRL. This work was supported by the National Natural Science Foundation of China (No. 12404075, No. 12274329), and the Hubei Provincial Natural Science Foundation of China (Grant No. 2024AFB935).

References

[1] L. Fu and C. L. Kane, Superconducting Proximity Effect and Majorana Fermions at the Surface of a Topological Insulator, Phys. Rev. Lett. **100**, 096407 (2008).

[2] M.-X. Wang, C. Liu, J.-P. Xu, F. Yang, L. Miao, M.-Y. Yao, C. L. Gao, C. Shen, X. Ma, X. Chen et al., The Coexistence of Superconductivity and Topological Order in the Bi_2Se_3 Thin Films, Science **336**, 52 (2012).

[3] V. Mourik, K. Zuo, S. M. Frolov, S. R. Plissard, E. P. A. M. Bakkers, and L. P. Kouwenhoven, Signatures of Majorana Fermions in Hybrid Superconductor-Semiconductor Nanowire Devices, Science **336**, 1003 (2012).

[4] S.-Y. Xu, N. Alidoust, I. Belopolski, A. Richardella, C. Liu, M. Neupane, G. Bian, S.-H. Huang, R. Sankar, C. Fang et al., Momentum-space imaging of Cooper pairing in a half-Dirac-gas topological superconductor, Nat. Phys. **10**, 943 (2014).

[5] R. M. Lutchyn, E. P. a. M. Bakkers, L. P. Kouwenhoven, P. Krogstrup, C. M. Marcus, and Y. Oreg, Majorana zero modes in superconductor–semiconductor heterostructures, Nat. Rev. Mater. **3**, 52 (2018).

[6] S. M. Albrecht, A. P. Higginbotham, M. Madsen, F. Kuemmeth, T. S. Jespersen, J. Nygård, P. Krogstrup, and C. M. Marcus, Exponential protection of zero modes in Majorana islands, Nature **531**, 206 (2016).

[7] L. A. Wray, S.-Y. Xu, Y. Xia, Y. S. Hor, D. Qian, A. V. Fedorov, H. Lin, A. Bansil, R. J. Cava, and M. Z. Hasan, Observation of topological order in a superconducting doped topological insulator, Nat. Phys. **6**, 855 (2010).

[8] P. Zhang, K. Yaji, T. Hashimoto, Y. Ota, T. Kondo, K. Okazaki, Z. Wang, J. Wen, G. D. Gu, H. Ding et al., Observation of topological superconductivity on the surface of an iron-based superconductor, Science **360**, 182 (2018).

[9] Q. Liu, C. Chen, T. Zhang, R. Peng, Y.-J. Yan, C.-H.-P. Wen, X. Lou, Y.-L. Huang, J.-P. Tian, X.-L. Dong et al., Robust and Clean Majorana Zero Mode in the Vortex Core of High-Temperature Superconductor $(Li_{0.84}Fe_{0.16})$OHFeSe, Phys. Rev. X **8**, 041056 (2018).

[10] Y. Yuan, J. Pan, X. Wang, Y. Fang, C. Song, L. Wang, K. He, X. Ma, H. Zhang, F. Huang et al., Evidence of anisotropic Majorana bound states in 2M-WS_2, Nat. Phys. **15**, 1046 (2019).

[11] Y. W. Li, H. J. Zheng, Y. Q. Fang, D. Q. Zhang, Y. J. Chen, C. Chen, A. J. Liang, W. J. Shi, D. Pei, L. X. Xu et al., Observation of topological superconductivity in a stoichiometric transition metal dichalcogenide 2M-WS_2, Nat. Commun. **12**, 2874 (2021).

[12] Z. Lai, Q. He, T. H. Tran, D. V. M. Repaka, D.-D. Zhou, Y. Sun, S. Xi, Y. Li, A. Chaturvedi, C. Tan et al., Metastable 1T′-phase group VIB transition metal dichalcogenide crystals, Nat. Mater. **20**, 8 (2021).

[13] Y. Yang, Q. Tao, Y. Fang, G. Tang, C. Yao, X. Yan, C. Jiang, X. Xu, F. Huang, W. Ding et al., Anomalous enhancement of the Nernst effect at the crossover between a Fermi liquid and a strange metal, Nat. Phys. **19**, 379 (2023).

[14] X. Che, Y. Deng, Y. Fang, J. Pan, Y. Yu, and F. Huang, Gate-Tunable Electrical Transport in Thin 2M-WS_2 Flakes, Adv. Electron. Mater. **5**, 1900462 (2019).

[15] C. Zhao, X. Che, Z. Zhang, and F. Huang, P-type doping in 2M-WS2 for a complete phase diagram, Dalton Trans. **50**, 3862 (2021).

[16] L. Xu, Y. Li, Y. Fang, H. Zheng, W. Shi, C. Chen, D. Pei, D. Lu, M. Hashimoto, M. Wang et al., Topology Hierarchy of Transition Metal Dichalcogenides Built from Quantum Spin Hall Layers, Adv. Mater. **35**, 2300227 (2023).

[17] Y. Li, L. Xu, G. Liu, Y. Fang, H. Zheng, S. Dai, E. Li, G. Zhu, S. Zhang, S. Liang et al., Evidence of strong and mode-selective electron–phonon coupling in the topological superconductor candidate 2M-WS_2, Nat. Commun. **15**, 6235 (2024).

[18] Y. Fang, J. Pan, D. Zhang, D. Wang, H. T. Hirose, T. Terashima, S. Uji, Y. Yuan, W. Li, Z. Tian et al., Discovery of Superconductivity in 2M WS_2 with Possible Topological Surface States, Adv. Mater. **31**, 1901942 (2019).

[19] H. Zhang, C.-X. Liu, X.-L. Qi, X. Dai, Z. Fang, and S.-C. Zhang, Topological insulators in Bi_2Se_3, Bi_2Te_3 and Sb_2Te_3 with a single Dirac cone on the surface, Nat. Phys. **5**, 438 (2009).

[20] Y. Xia, D. Qian, D. Hsieh, L. Wray, A. Pal, H. Lin, A. Bansil, D. Grauer, Y. S. Hor, R. J. Cava et al., Observation of a large-gap topological-insulator class with a single Dirac cone on the surface, Nat. Phys. **5**, 398 (2009).

[21] Y. L. Chen, J. G. Analytis, J.-H. Chu, Z. K. Liu, S.-K. Mo, X. L. Qi, H. J. Zhang, D. H. Lu, X. Dai, Z. Fang et al., Experimental Realization of a Three-Dimensional Topological Insulator, Bi_2Te_3, Science **325**, 178 (2009).

[22] P. Zhang, J.-Z. Ma, Y. Ishida, L.-X. Zhao, Q.-N. Xu, B.-Q. Lv, K. Yaji, G.-F. Chen, H.-M. Weng, X. Dai et al., Topologically Entangled Rashba-Split Shockley States on the Surface of Grey Arsenic, Phys. Rev. Lett. **118**, 046802 (2017).

[23] S. Cho, S. Huh, Y. Fang, C. Hua, H. Bai, Z. Jiang, Z. Liu, J. Liu, Z. Chen, Y. Fukushima et al., Direct Observation of the Topological Surface State in the Topological Superconductor 2M-WS_2, Nano Lett. **22**, 8827 (2022).

[24] H. Gao, H. Xiao, F. Wang, F. Zhu, M. Wang, Z. Liu, Y. Chen, and C. Chen, Nano-ARPES Endstation at BL07U of Shanghai Synchrotron Radiation Facility, Synchrotron Radiation News **37**, 12 (2024).

[25] M. Hashimoto, Y. Zhong, and D. Lu, Oxide MBE – ARPES at SSRL Beamline 5-2, Synchrotron Radiation News **37**, 4 (2024).

[26] G. Kresse and J. Furthmüller, Efficient iterative schemes for ab initio total-energy calculations using a plane-wave basis set, Phys. Rev. B **54**, 11169 (1996).

[27] J. P. Perdew, K. Burke, and M. Ernzerhof, Generalized Gradient Approximation Made Simple, Phys. Rev. Lett. **77**, 3865 (1996).

[28] Q. Wu, S. Zhang, H. F. Song, M. Troyer, and A. A. Soluyanov, WannierTools: An open-source software package for novel topological materials, Comput. Phys. Commun. **224**, 405 (2018).

[29] N. Marzari and D. Vanderbilt, Maximally localized generalized Wannier functions for composite energy bands, Phys. Rev. B **56**, 12847 (1997).

[30] A. A. Mostofi, J. R. Yates, G. Pizzi, Y. S. Lee, I. Souza, D. Vanderbilt, and N. Marzari, An updated version of wannier90: A tool for obtaining maximally-localised Wannier functions, Comput. Phys. Commun. **185**, 2309 (2014).

[31] I. Souza, N. Marzari, and D. Vanderbilt, Maximally localized Wannier functions for entangled energy bands, Phys. Rev. B **65**, 035109 (2001).

[32] W. Kohn and L. J. Sham, Self-Consistent Equations Including Exchange and Correlation Effects, Phys. Rev. **140**, A1133 (1965).

[33] A. D. Becke and E. R. Johnson, A simple effective potential for exchange, J. Chem. Phys. **124** 124, 221101 (2006).

[34] A. V. Krukau, O. A. Vydrov, A. F. Izmaylov, and G. E. Scuseria, Influence of the exchange screening parameter on the performance of screened hybrid functionals, J. Chem. Phys.**125**, 224106 (2006).

[35] See Supplemental Material for more detailed ARPES data and calculations.

[36] M. Chhowalla, H. S. Shin, G. Eda, L.-J. Li, K. P. Loh, and H. Zhang, The chemistry of two-dimensional layered transition metal dichalcogenide nanosheets, Nat. Chem. **5**, 263 (2013).

[37] J. C. Y. Teo, L. Fu, and C. L. Kane, Surface states and topological invariants in three-dimensional topological insulators: Application to $Bi_{1-x}Sb_x$, Phys. Rev. B **78**, 045426 (2008).

[38] M. Z. Hasan and C. L. Kane, Colloquium: Topological insulators, Rev. Mod. Phys. **82**, 3045 (2010).

[39] P. Zhang, R. Noguchi, K. Kuroda, C. Lin, K. Kawaguchi, K. Yaji, A. Harasawa, M. Lippmaa, S. Nie, H. Weng, V. Kandyba et al., Observation and control of the weak topological insulator state in $ZrTe_5$, Nat. Commun. 12, 406 (2021).

[40] C. Lin, M. Ochi, R. Noguchi, K. Kuroda, M. Sakoda, A. Nomura, M. Tsubota, P. Zhang, C. Bareille, K. Kurokawa et al., Visualization of the strain-induced topological phase transition in a quasi-one-dimensional superconductor $TaSe_3$, Nat. Mater. **20**, 1093 (2021).

[41] Y. Fang, Q. Dong, J. Pan, H. Liu, P. Liu, Y. Sun, Q. Li, W. Zhao, B. Liu, and F. Huang, Observation of superconductivity in pressurized 2M WSe_2 crystals, J. Mater. Chem. C 7, 8551 (2019).

[42] Z. Guguchia, D. J. Gawryluk, M. Brzezinska, S. S. Tsirkin, R. Khasanov, E. Pomjakushina, F. O. von Rohr, J. A. T. Verezhak, M. Z. Hasan, T. Neupert et al., Nodeless superconductivity and its evolution with pressure in the layered dirac semimetal 2M-WS_2, Npj Quantum Mater. **4**, 1 (2019).

[43] P. Zhang, Z. Wang, X. Wu, K. Yaji, Y. Ishida, Y. Kohama, G. Dai, Y. Sun, C. Bareille, K. Kuroda et al., Multiple topological states in iron-based superconductors, Nat. Phys **15**, 41 (2019).

[44] N. Avraham, A. Kumar Nayak, A. Steinbok, A. Norris, H. Fu, Y. Sun, Y. Qi, L. Pan, A. Isaeva, A. Zeugner et al., Visualizing coexisting surface states in the weak and crystalline topological insulator Bi_2TeI, Nat. Mater. **19**, 610 (2020).

[45] M. Eschbach, M. Lanius, C. Niu, E. Młyńczak, P. Gospodarič, J. Kellner, P. Schüffelgen, M. Gehlmann, S. Döring, E. Neumann et al., Bi1Te1 is a dual topological insulator, Nat. Commun. **8**, 14976 (2017).

[46] I. Cucchi, A. Marrazzo, E. Cappelli, S. Riccò, F. Y. Bruno, S. Lisi, M. Hoesch, T. K. Kim, C. Cacho, C. Besnard et al., Bulk and Surface Electronic Structure of the Dual-Topology Semimetal Pt_2HgSe_3, Phys. Rev. Lett. **124**, 106402 (2020).

[47] D.-Y. Wang, Q. Jiang, K. Kuroda, K. Kawaguchi, A. Harasawa, K. Yaji, A. Ernst, H.-J. Qian, W.-J. Liu, H.-M. Zha et al., Coexistence of Strong and Weak Topological Orders in a Quasi-One-Dimensional Material, Phys. Rev. Lett. **129**, 146401 (2022).

[48] X.-B. Shi, P. He, and W.-W. Zhao, Dual topology in van der Waals-type superconductor Nb_2S_2C, Tungsten **5**, 357 (2023).

[49] L. X. Xu, Y. Y. Y. Xia, S. Liu, Y. W. Li, L. Y. Wei, H. Y. Wang, C. W. Wang, H. F. Yang, A. J. Liang, K. Huang et al., Evidence of a topological edge state in a superconducting nonsymmorphic nodal-line semimetal, Phys. Rev. B **103**, L201109 (2021).

[50] Z. Huang, W. L. Liu, H. Y. Wang, Y. L. Su, Z. T. Liu, X. B. Shi, S. Y. Gao, Z. Y. Chen, Y. J. Yan, Z. C. Jiang et al., Dual topological states in the layered titanium-based oxypnictide superconductor $BaTi_2Sb_2O$, Npj Quantum Mater. **7**, 1 (2022).

[51] L. Fu and C. L. Kane, Topological insulators with inversion symmetry, Phys. Rev. B **76**, 045302 (2007).

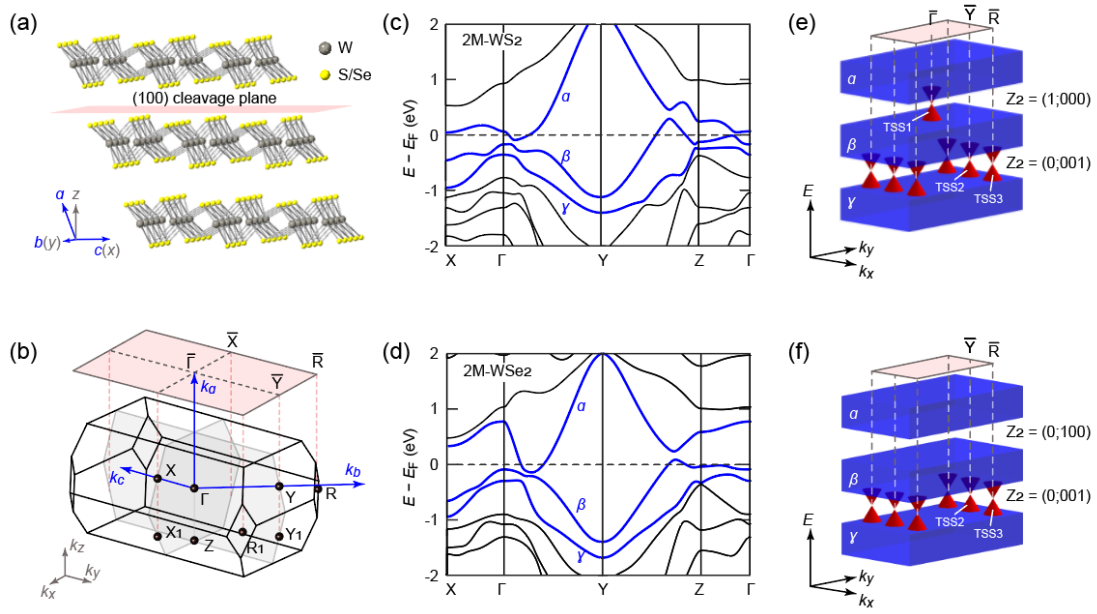

FIG. 1. (a) Crystal structure of 2M-phase WS_2 and WSe_2 with its naturally cleaved (100) plane, indicated by the red surface. (b). Bulk Brillouin zone (BZ) with time-reversal invariant momenta marked and (100) projected surface BZ indicated by the red rectangle. (c) and (d) Calculated bulk band structure of 2M-WS_2 (c) and 2M-WSe_2 (d). SOC is included. The α, β and γ bands highlighted by the blue lines are three bands near the Fermi level. (e) and (f) Possible connecting configurations of topological surface Dirac cones among the α, β, and γ bulk continuums in 2M-WS_2 (e) and 2M-WSe_2 (f), respectively.

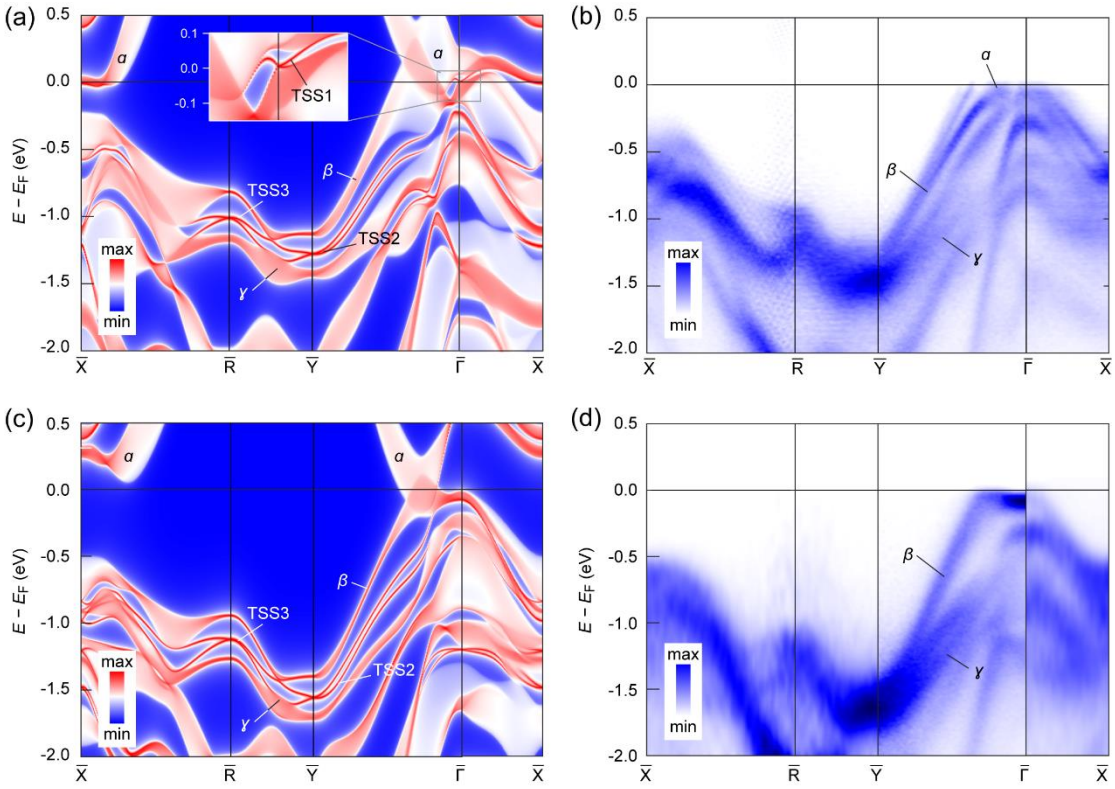

FIG. 2. (a) and (c) (100) surface-projected band calculations of 2M-WS_2 (a) and 2M-WSe_2 (c) along the $\overline{X}-\overline{R}-\overline{Y}-\overline{\Gamma}-\overline{X}$ direction. The α, β, and γ bulk continuums and TSS1, TSS2, and TSS3 are indicated. The inset in (a) is a zoom-in plot of TSS1. (b) and (d) Corresponding synchrotron-ARPES measured band dispersions of (a) and (c), respectively.

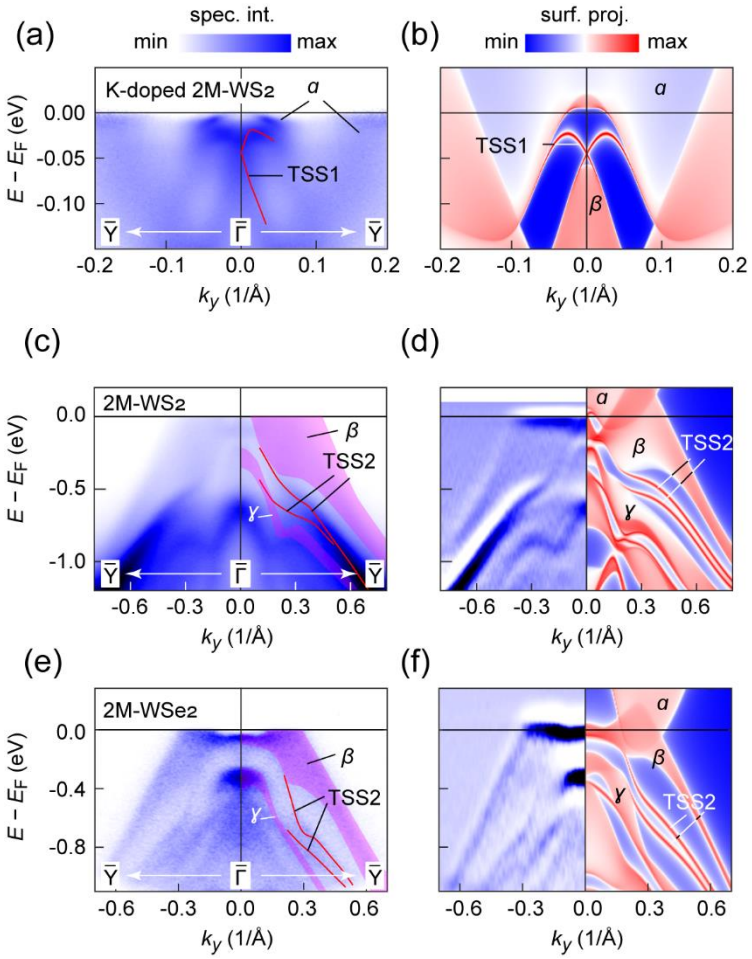

FIG. 3. (a) Laser-ARPES measured band dispersion of TSS1 along the $\overline{Y}-\overline{\Gamma}-\overline{Y}$ direction of K-doped 2M-WS_2. (b) Corresponding calculation of (a). (c) Synchrotron-ARPES measured band dispersion of TSS2 along the $\overline{Y}-\overline{\Gamma}-\overline{Y}$ direction of pristine 2M-WS_2 under $h\nu$ = 28 eV. (d) Corresponding second-derivative plot (left panel) and calculation (right panel) of (c). (e) Synchrotron-ARPES measured band dispersion of TSS2 along the $\overline{Y}-\overline{\Gamma}-\overline{Y}$ direction of pristine 2M-WSe_2 under $h\nu$ = 94 eV. (f) Corresponding second-derivative plot (left panel) and calculation (right panel) of (e). TSS are indicated by red lines and bulk band continuums are indicated by magenta-shaded areas.

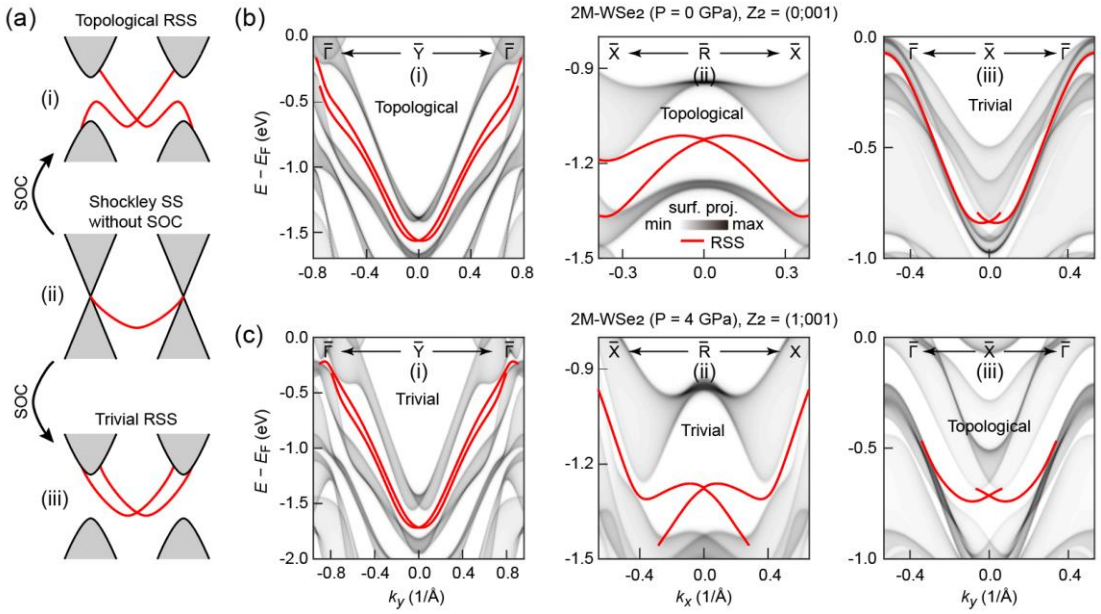

FIG. 4. (a) Band illustrations of topological RSS (upper panel) and trivial RSS (lower panel) derived from the Shockley surface states (middle panel) by introducing SOC. (b) Bulk and surface band calculations of 2M-WSe_2 under zero pressure along $\bar{\Gamma} - \bar{Y} - \bar{\Gamma}$ (left panel), $\bar{X} - \bar{R} - \bar{X}$ (middle panel), and $\bar{\Gamma} - \bar{X} - \bar{\Gamma}$ (right panel). (c) Same as (b) but under 4-GPa pressure. The bulk continuums are indicated by the gray-shaded areas and the RSS are indicated by red lines. Z_2 invariant (the curved Fermi level is set between the β and γ bands), topological and trivial RSS are indicated in (b) and (c).